Bio-Design and Manufacturing (2022) 5:700–713
https://doi.org/10.1007/s42242-022-00197-0

RESEARCH ARTICLE

Laser-induced jigsaw-like graphene structure inspired by *Oxalis corniculata Linn.* leaf

Wentao Wang[1] · Longsheng Lu[1] · Xiaoyu Lu[1] · Zhanbo Liang[1] · Biao Tang[2] · Yingxi Xie[1]

Received: 15 October 2021 / Accepted: 10 March 2022 / Published online: 14 June 2022

Abstract

The laser scribing of polyimide (PI, Kapton) film is a new, simple and effective method for graphene preparation. Moreover, the superhydrophobic surface modification can undoubtedly widen the application fields of graphene. Herein, inspired by the hydrophobic and self-cleaning properties of natural *Oxalis corniculata Linn.* leaves, we propose a novel bionic manufacturing method for superhydrophobic laser-induced graphene (LIG). By tailoring the geometric parameters (size, roughness and height/area ratio) and chemical composition, the three-dimensional (3D) multistage LIG, i.e., with micro-jigsaw-like and porous structure, can deliver a static water contact angle (WCA) of 153.5° ± 0.6°, a water sliding angle (WSA) of 2.5° ± 0.5°, and great superhydrophobic stability lasting for 100 days (WCAs ≈ 150°). This outstanding water repellency is achieved by the secondary structure of jigsaw-like LIG, a porous morphology that traps air layers at the solid–liquid interface. The robust self-cleaning and anti-stick functions of 3D bionic and multistage LIG are demonstrated to confirm its great potential in wearable electronics.

Graphic abstract

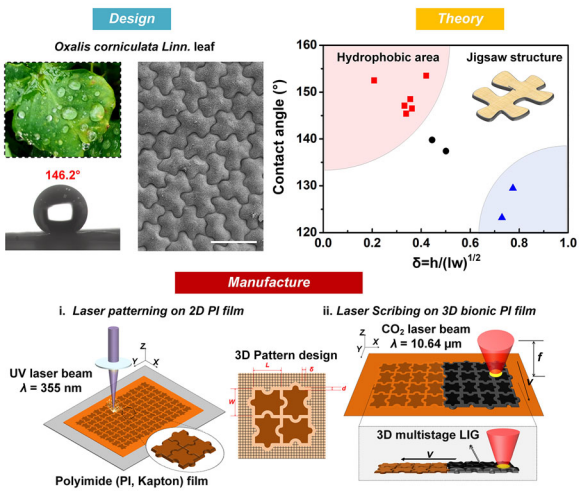

Keywords Laser-induced graphene · *Oxalis corniculata Linn.* · Bionic · Multistage structure · Superhydrophobic surface

Introduction

The latest research has witnessed the in situ synthesis of graphene by laser scribing on a variety of carbon precursors, including synthetic polymers, renewable resources and even non-polymer materials [1, 2]. Unlike the conventional graphene preparation method that requires high-temperature

✉ Yingxi Xie
xieyingxi@scut.edu.cn

1 School of Mechanical and Automotive Engineering, South China University of Technology, Guangzhou 510641, China

2 Guangdong Provincial Key Laboratory of Optical Information Materials and Technology, South China Normal University, Guangzhou 510006, China

treatment, specific atmospheric conditions or a multi-step chemical route, laser scribing technology enables a one-step, mask free and on-demand preparation of graphene with high-spatial and large-area patterns [3–5]. The resulting product, known as laser-induced graphene (LIG), has typical three-dimensional (3D) porous structure with pore sizes ranging from nanometer- to micron-scale [6]. The large specific surface area and conductivity of LIG make it widely used in flexible energy collection [7], storage [8] and sensor devices [9].

As the key component of flexible electronic devices, LIG has long been subject to improvements in the physical, chemical and electrical properties [10]. Moreover, due to its high surface roughness, low density and non-polar carbon structure, it is also an ideal candidate for the preparation of superhydrophobic surfaces [11]. This feature, for the most part, can add some ancillary functionality to future LIG-based applications [12]. For instance, by optimizing the wettability of LIG electrode, the superhydrophobic surface can prevent sweat or external liquids such as rain from entering the inner circuit, thus improving the stability and robustness of electronic skin [13, 14]. As for LIG-assembled nanogenerators, the rapid sliding of water droplets upon slight contact with the superhydrophobic surface facilitates carrier migration and charge generation [7, 15].

In order to improve the water repellency of graphene, the initial strategies have relied mainly on coating deposition, or the introduction of functional groups with low surface energy [16, 17]. Nonetheless, the key drawback of these methods is that the toxic ingredients in wearable electronics are harmful to health when they come into close contact with human skin [18]. Recent studies have shown that the superhydrophobic behavior of LIG can be realized by polymer infiltration [19], micro-/nanostructure construction (by changing the laser parameters) or modification in specific atmospheres (N_2, H_2 and Ar) [11, 20]. Wang et al. proposed a defocusing and grafting strategy to prepare LIG with tunable wettability from superhydrophilicity to superhydrophobicity for various liquids [21]. Nasser et al. demonstrated the direct spatial printing of surfaces with either superhydrophilic or superhydrophobic characteristics by simple control over the LIG array morphology [22]. In spite of the above efforts, the redundant post-processing steps or atmosphere chambers run counter to the rapid, large-area, and easy-to-operate manufacturing concept of laser scribing technology, greatly limiting the long-term development of LIG [23, 24].

Over the course of evolution, many creatures have developed unique abilities under the great pressure to survive, and hydrophobicity has naturally become one of their great charms [25–28]. In the case of a lotus leaf, rain and dew can roll over its superhydrophobic leaves to remove dust, so as not to affect photosynthesis [29–31]. Kingfishers can easily change direction in heavy rain, dive into the water to catch prey and take off again thanks to the oily substance they rub into their feathers [32]. The surface dehydration state of these living things is well-known as a synergistic effect of multiple dynamic factors, including non-polar wax coating and micro–nano-surface structures [31, 33, 34]. Using such a biological blueprint as a template, the bionic LIG surface can be designed in a simple and efficient way to realize the hydrophobic functions.

Oxalis corniculata Linn. is a widely distributed genus of wood sorrels, which are highly successful for their ability to propagate through vegetative reproduction. These herbs prefer a sunny, warm and humid environment; the surface hydrophobicity of their leaves avoids water accumulation and thus increases photosynthetic yield. In this study, inspired by the micro-/nano-surface of *Oxalis corniculata Linn.* leaves (showing an interesting jigsaw-like pattern), we firstly graphically etched the pure polyimide (PI) film with 355 nm ultraviolet (UV) laser and then fabricated a bionic LIG surface on it by CO_2 laser scribing. To the best of our knowledge, it is the first time that 3D porous LIG was manufactured in situ in a bionic manner to attain superhydrophobic characteristics. By tailoring the 3D multistage structure, i.e., the micro-jigsaw-like surface and porous LIG, as well as the chemical composition, the LIG bionic surface could deliver a static water contact angle (WCA) of $153.5° \pm 0.6°$, a water sliding angle (WSA) of $2.5° \pm 0.5°$ and great superhydrophobic stability lasting for 100 days (WCA $\approx 150°$). The robust self-cleaning and waterproof functions of 3D multistage LIG electrode further demonstrated a great potential in future biomedical fields, such as preventing water and blood from sticking to medical electrodes and devices.

Experimental section

Materials and processing parameters

Oxalis corniculata Linn. leaves were collected from the grounds of South China University of Technology (SCUT). The PI film (DuPont Kapton® HN, thickness: 125 μm) was washed with absolute ethanol and then dried in a vacuum oven at 90 °C. The jigsaw-like structure of LIG was fabricated in two steps. Firstly, a UV laser cutting system ($\lambda = 355$ nm, LT20, Latuo Laser Equipment Co., Ltd., China) was used to etch the pure PI film with jigsaw-like patterns. Then, the laser scribing of 3D bionic LIG electrodes was carried out on a continuous-wave CO_2 laser cutting system ($\lambda = 10.64$ μm, XB4060, Xinbang Laser Equipment Co., Ltd., China) with a minimum spot diameter of about 120 μm and a maximum output power of 10 W. The scanning interval was adjusted to 50 μm, so that the whole PI film could be fully scanned and carbonized. Notably, a small amount of carbonization products was removed with ethanol, and the PI film was cleaned prior to the in situ generation of LIG.

The size, structure and chemical composition of the bionic LIG structure were adjusted by two controllable parameters, namely laser power P and focusing distance d. The 3D bionic LIG was prepatterned and then in situ generated under photothermal transition. Then, we focused on investigating the influence of structural parameters on the surface wettability of bionic LIG.

Characterization

A field emission scanning electron microscope (SEM, ZEISS Merlin) was used to examine the surface morphology of jigsaw-like LIG electrode and *Oxalis corniculata Linn.* leaves. The plant samples were freeze-dried and dehydrated in a high-vacuum environment to prevent moisture from evaporating. This may have a negative effect and lead to sample deformation and instrument damage. To fix the original morphology, the leaves were rinsed with deionized water to remove contaminants and permeated in 2.5% glutaraldehyde for 4 h. The samples were separately soaked in 30%, 50%, 70%, 90% and 100% ethanol for 15 min for gradient dehydration.

Raman spectroscopy (Lab Ram HR800, 50× objective, laser spot size < 10 μm) was employed to measure the carbonization degree of LIG. The surface profiles of samples prepared with different parameters were investigated using a 3D super depth of field digital microscope (VH-Z100R, Keyence Corp., Japan). A scanning X-ray microprobe (XPS, Quantera SXM, PHI) was employed to analyze the element component and valence state. The powders scraped from LIG samples were characterized by a transmission electron microscope (TEM, JEOL 2100F). The SEM, Raman and XPS characterizations were performed directly on the LIG layers of PI films.

Measurement of surface wettability

A contact angle measuring instrument (JC2000D1, Powereach®, China) was used to measure the static WCAs in six different locations of the samples via the sessile drop method with about 5 μL water. The WSAs were determined by the tilting plate method. The WCAs were recorded after the droplet stabilized for 60 s. During the test, the room temperature and relative humidity were controlled at 24 °C and 60%, respectively, to reduce the environmental effects.

The bouncing effect of microdroplets was tested using 5 μL water droplet as a carrier. The bionic surface of LIG was coated with 20 g micron copper powder and then completely washed with water to demonstrate its self-cleaning effect. The LIG sample was dipped in a beaker of 300 mL deionized water to display its anti-stick properties. All of the supplementary videos were recorded using an optical tensiometer (BQ2000PW, Great Wall®, China).

Results and discussion

Morphic groups and their structural properties

Oxalis corniculata Linn. is a large genus of wood sorrel species with strong reproductive capacities, which includes subtropical plants. Similar to lotus leaves, after rain, *Oxalis corniculata Linn.* leaves are not wetted given their hydrophobicity and self-cleaning properties. Dust on leaves is carried away by raindrops; hence, photosynthesis can function normally and sustain primary production (Fig. 1a). Out of curiosity, the wettability of *Oxalis corniculata Linn.* leaves was tested, and its static WCA was found as 146.2° ± 2.1°, indicating its natural hydrophobic properties (Fig. 1b). According to previous studies, hydrophobic leaves often exhibit micro–nano-surface structures and are covered with a cuticle or villi to ensure low surface energy. Interestingly, herein, the SEM image (Fig. 1c) shows that the surface topography of *Oxalis corniculata Linn.* leaves is composed of irregular jigsaw-like microstructures, similar to a jigsaw puzzle played by children (Fig. 1d). The enlarged morphology (Figs. 1e and 1f) demonstrated that each jigsaw-like microstructure is decorated with protruding blade-like fragments with an average length of about 1 μm. Moreover, there are nanowax layers deposited on the microfragments. Due to the synergy of multistage structures, including jigsaw microstructures, microfragments and nanowax layers, once the droplets touch the leaf, they will immediately roll off its surface. As described by the Cassie–Baxter model, air supported by the composite surface of leaves is trapped between the microstructure and droplets.

As schematically illustrated in Fig. 2a, inspired by the jigsaw-like morphology of *Oxalis corniculata Linn.* leaves, we first used a 355 nm UV laser to design the bionic structure on the PI film. Then, CO_2 laser scribing on the 3D PI film was undertaken to obtain the bottom-up growth of LIG. The standard jigsaw-like LIG structure was arranged to form a multistage array. The UV laser etching process was mainly used to define the contour of a jigsaw-like LIG, while CO_2 laser scribing was carried out in the whole area. The final morphology is related to several parameters of laser. Here, linear heat density (LHD, unit: J/mm) is introduced to describe the heating level, which is quantified by the amount of heat injected into a unit length along the scanning direction [35]:

$$\mathrm{LHD} = P/v, \tag{1}$$

where P represents the laser power, and v represents the scanning rate. Therefore, we controlled the key factors of LDH and focusing distance d in the CO_2 laser scribing process to adjust the structure–wettability relationship of 3D bionic LIG (Fig. 2b), which will be fully discussed later.

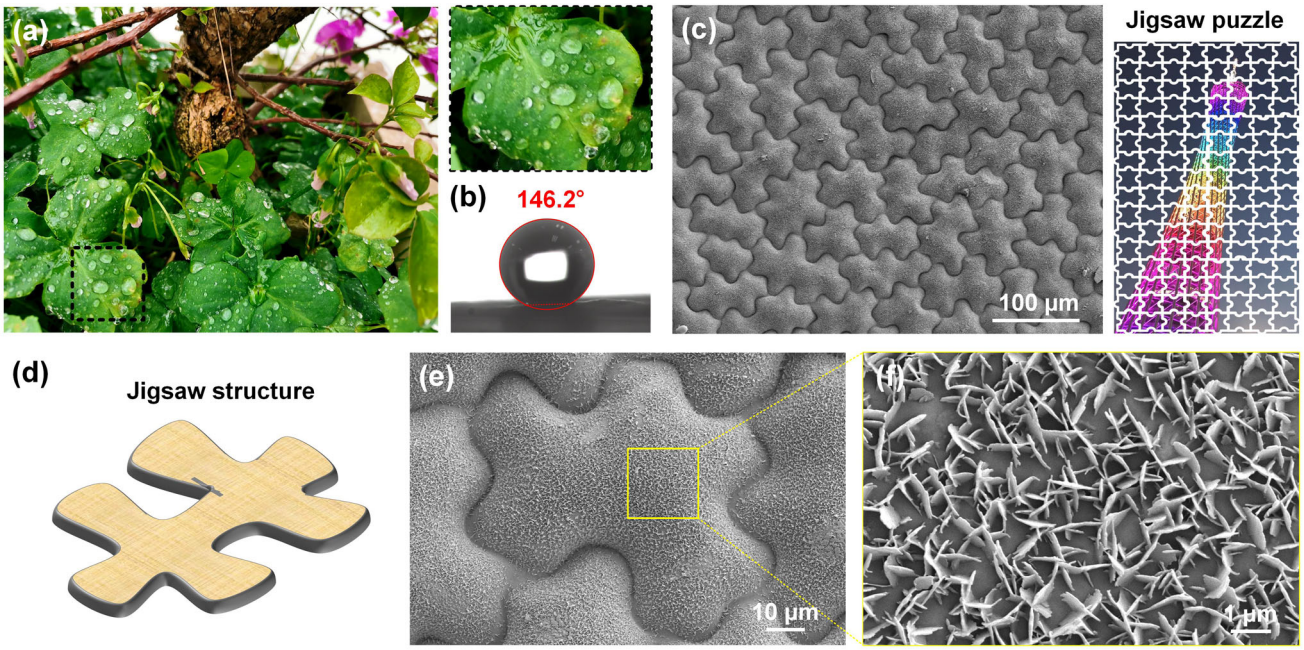

Fig. 1 **a** The *Oxalis corniculata Linn.* leaves are not wetted due to hydrophobicity and self-cleaning after rain. **b** *Oxalis corniculata Linn.* leaves showing natural hydrophobicity with a static WCA of 146.2° ± 2.1°. **c** The surface topography of *Oxalis corniculata Linn.* leaves features irregular jigsaw-like microstructures. **d** Schematic diagram of a jigsaw structure that is similar to the surface morphology. **e** SEM image showing the multistage characteristic of a jigsaw-like microstructure decorated with protruding blade-like fragments, and **f** enlarged view displaying fragments that are evenly embedded across the surface with an average length of about 1 μm

As shown in Fig. 2c, after UV laser etching, the PI film presents an evenly distributed jigsaw-like surface. Most of substrate is directly vaporized at high temperature, and a small amount of carbonization is cleaned by ethanol without any residue. Unlike the previous reported superhydrophobic LIG, we used the laser-etched PI film with 3D bionic structure as a carbon precursor [36, 37]. Therefore, LIG grows from bottom-to-top through CO_2 laser scribing into a 3D multistage structure. Under the optimum laser scribing parameters, namely, an LDH of 0.05 J/mm at on-focus condition, the jigsaw-like pattern on LIG with bionic unit size of about 200 μm and microscale gaps of about 100 μm is regularly arranged on the surface (Fig. 2d).

Due to the coupling effects of absorption, refraction and reflection of CO_2 light beam, an interesting behavior was observed in the 3D bionic structure. The LIG probably follows a bottom-up growth mechanism during laser scribing; hence, we measured three locations of a jigsaw-like unit (regions i, ii and iii) and found that they exhibited different morphologies [38]. At the top, due to the sufficient heat accumulation and rapid gas release, LIG displays a typical porous structure (Fig. 2e). Meanwhile, from center to edge of the jigsaw-like unit, the porous morphology tends to be closed.

The 3D topography of LIG bionic surface is depicted in Fig. 2f, where the height between the valley and peak of jigsaw-like units is about 195.3 μm, and the valley width is about 98.4 μm. It is worth noting that the topography can be tailored by setting the different processing parameters, resulting from the multi-physical interaction between 3D PI film and laser beam. This uniform and multistage morphology, including micron-scale bionic structure and porous LIG, plays a key role in capturing the air phase at the liquid–solid interface [39]. This exciting structure agrees well with the multistage surface of *Oxalis corniculata Linn.* leaves, suggesting that the novel method of laser scribing on 3D PI film is a promising, highly realistic and customizable method for bionic manufacturing [40].

Raman spectroscopy was used to confirm the carbonization degree within a single jigsaw-like LIG unit. A total of three main bands, namely D peak (about 1350 cm^{-1}), G peak (about 1580 cm^{-1}), and 2D peak (about 2690 cm^{-1}), can be clearly observed in Fig. 2g. As shown in Fig. S1 (Supplementary Information), the ratio of D peak and G peak (I_D/I_G) represents the defect density of graphene, and the ratio of 2D peak and G peak (I_{2D}/I_G), as well as the full width at half maximum (FWHM), can effectively indicate the number of graphene layers [41, 42]. Two sharp D and G peaks with a relatively low-intensity ratio of I_D/I_G and FWHM(G) are obtained in the top area, indicating the formation of high-quality LIG during the photothermal reaction [43]. The increase of I_D/I_G and FWHM(G) indicates that more defects exist in the middle and bottom area of LIG, which is consistent with the surface topography.

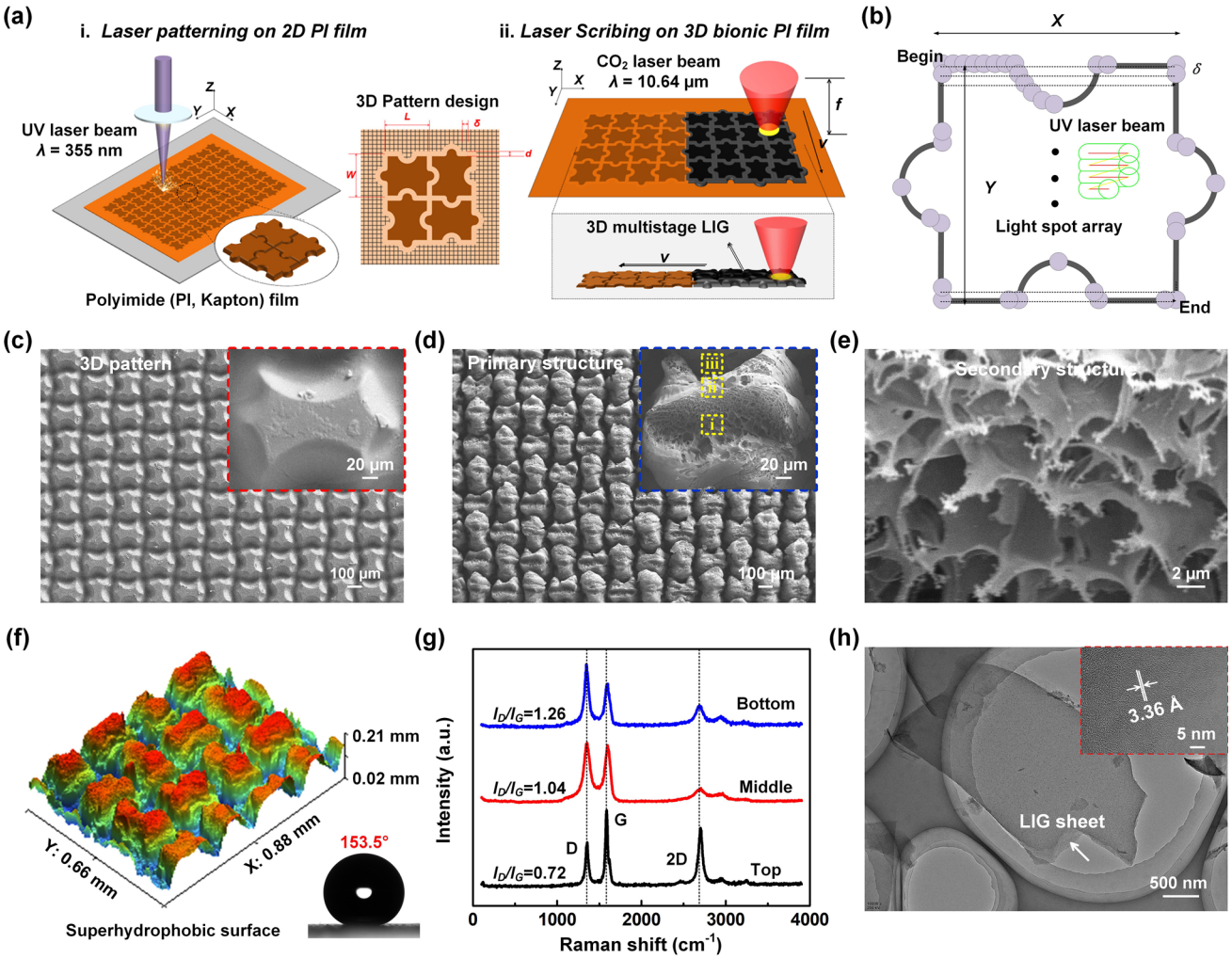

Fig. 2 **a** Schematic illustration of a jigsaw-like LIG fabricated by laser patterning on pure PI film and then laser scribing on a 3D bionic PI film. **b** UV laser etching is mainly performed to scribe the contour of a jigsaw-like LIG, and CO_2 laser scribing is carried out in the whole area. **c** SEM image of a pure PI film etched by a UV laser, with the magnified image insert showing a standard 3D bionic structure similar to the surface morphology of *Oxalis corniculata Linn.* leaves. **d** The laser scribing process of jigsaw-like LIG on 3D bionic PI film followed by a bottom-up growth mechanism. The image insert shows the 3D multistage morphology with different local structures in the top area (regions i, ii, and iii). **e** Region i shows the secondary structure of a typical porous LIG. **f** The 3D topography of jigsaw-like structural LIG arranged in the *x*- and *y*-directions with uniform morphology. **g** Raman spectra of three regions in a single jigsaw-like LIG unit and its intensity ratio of I_D/I_G. **h** TEM image of jigsaw-like structural LIG with few-layer features, where the average lattice space of 3.36 Å confirms the existence of graphene

Micro-/nanoflakes of the jigsaw-like structural LIG with fewer layers can be clearly seen in the TEM image (Fig. 2h). In the enlarged images, from the edges of the flake, ripple-like wrinkled structures can be observed, which are caused by the thermal expansion in laser scribing. To show the periodicity and lattice stripes of graphene layers more clearly, TEM images of LIG at different magnifications are presented in Fig. S2 (Supplementary Information). The average lattice space of 3.36 Å (1 Å = 10^{-10} m) corresponds to the distance between two neighboring (002) planes in the graphitic materials [41].

Effects of laser parameters on surface morphology and wettability

As schematically illustrated in Fig. 3a, the laser scribing process of LIG bionic structure can be divided into two parts: the patterned etching of 2D plane PI film, and the bottom-to-top growth of LIG with 3D bionic surface. The etching and carbonization behaviors on the bionic surface are closely related to the laser–material interaction, among which beam characteristics and scribing parameters are the two main factors affecting the jigsaw-like structure of LIG [44].

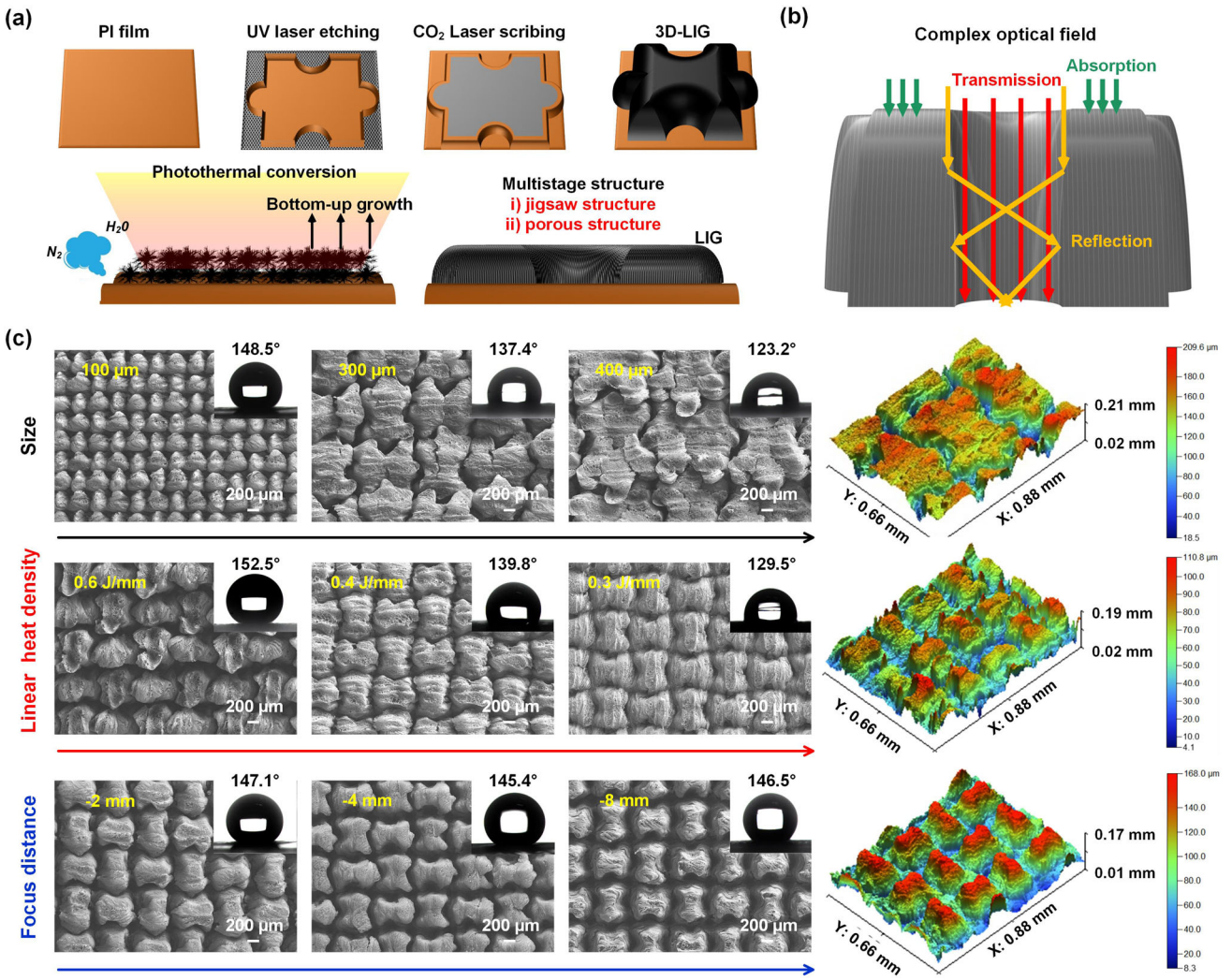

Fig. 3 **a** Schematic illustration of fabricating jigsaw-like structural LIG, whose multistage morphology was formed in a bottom-to-up manner during photothermal conversion. **b** Schematic diagram of a complex light field including the reflection, absorption, scattering, and transmission effects. **c** Surface morphology and WCAs of jigsaw-like structural LIG prepared with different parameters, including size, linear heat density and focus distance. The 3D topography of bionic units exhibits different heights, widths and lengths

Differently from previous work on the in situ generation of LIG on pure PI film, paper, wood and carbon cloth [5, 45–47], in the laser scribing of 3D PI film, a complex light field is the key to the preparation of multistage and jigsaw-like LIG (Fig. 3b). This has three particular reasons: (i) The light field is accompanied by an energy field, and it follows a Gaussian distribution, suggesting that the energy in the central region is much higher than that in the edge region [48]; (ii) The focal radius changes with focusing depth, so that the reflection, absorption, scattering and transmission would simultaneously occur in the light field; (iii) The LIG mostly follows the bottom-up growth mode on the 3D PI film, which further increases the differences in topographical morphology and carbonization ratio [49].

As for the typical porous structure of LIG, the CO_2 laser beam produces a local high-temperature zone of 1000–2000 K on the PI film. Thus, amorphous carbon, a disorganized mixture of all possible hybridizations, is fully converted into high-quality LIG with sp^2 C=C bond [50]. Carbonization on the 3D PI film can be regarded as a gasification process, which takes place over the surface at near sound speed, resulting in porous LIG with a jigsaw-like structure.

Subsequently, we further investigated the effects of LHD and d on the jigsaw-like surface. The height and top area (length and width) of a bionic unit were calculated to establish the structure–wettability relationship. As shown in Fig. 3c, using a relatively low LHD of 0.03 J/mm, LIG conversion

was not completed due to the insufficient laser energy. Some ignorable thermal deformations can be observed on the PI film, and the surface does not acquire a superhydrophobic characteristic. With a relatively higher LHD of 0.06 J/mm, the jigsaw-like LIG patterns were distorted due to excess heat energy and high-intensity impact. All of the morphologies of jigsaw-like structural LIG prepared under different LHD settings are illustrated in Fig. S3 (Supplementary Information). A superhydrophobic WCA of 152.5° ± 0.3° can be obtained due to the greater roughness of disordered surface and greatly increased C content, which will be discussed later.

The effects of size on bionic LIG morphology suggest that the jigsaw-like unit failed to form a normal shape below the standard scale of 200 μm. With the linear increase of size to 300 μm and then to 400 μm, the contours of jigsaw-like structure appeared, but WCAs decreased to 137.4° ± 1.4° and 123.2° ± 1.1°, respectively. These results are close to that of 108.2° ± 1.8° in the pure LIG layer and 57.9° ± 2.3° of LIG with a plain grid structure, suggesting that the influence of surface microstructure is gradually degrading (Figs. S4 and S5, Supplementary Information). In each sample, the upper part of the carbonization zone is smaller than the bottom area. The whole 3D topography of the sample is depicted in Fig. S6 (Supplementary Information), and the enlarged SEM images demonstrate the typical porous structure of LIG. The difference is that with the increase in size, the holes produced by air release become more uniform.

An appropriate adjustment of P and/or v enables the LHD of 0.05 J/mm to reach the carbonization threshold without exceeding the damage threshold. The heat energy followed by the photothermal mechanism could convert the 3D bionic surface into jigsaw-like structural LIG. A suitable bionic size of 200 μm in diameter could trap air and ensure a small contact area on the solid–liquid interface. Thus, the result of optimal bionic LIG is a high WCA of 153.5° ± 0.6°. The WSAs, stable wettability and its superhydrophobic applications will be discussed later.

In order to further explore the bionic structure–wettability relationship, another mild LIG conversion method is proposed, that is, increasing the laser spot size while maintaining the same LHD. Generally, when a laser beam is applied to PI film at a certain intensity, according to the Gaussian distribution, the maximum temperature is generated at the centerline of scanning trajectory. By defocusing the laser distance from Z-axis to focal plane, different anticipated spot sizes can be obtained, thus enhancing the exposure repetition rate per unit area. Under the same LHD, defocusing would generate a lower thermal load, resulting in mild carbonization. With the defocusing distance increasing from 2 to 4 cm and 8 cm, the topography (height, width and length) of the bionic units linearly decreases, but the spacing between adjacent structures is enlarged (Fig. S7, Supplementary Information). Interestingly, the WCAs of these samples do not change much (147.1° ± 0.8°, 145.4° ± 0.7° and 146.5° ± 0.8°), which is closely linked to the roughness and chemical composition of jigsaw-like structure, which will be discussed later. According to the above results, we can consider that the surface morphology of bionic LIG can be adjusted by changing the processing parameters to achieve a superhydrophobic effect.

The above-described method of obtaining stable WCAs on bionic LIG surface by laser defocusing has proved as highly promising. It is worth noting that the slight changes in contact angles can actually be explained by two different contact mechanisms, namely the Wenzel model and the Cassie–Baxter model. In the absence of laser defocusing, the porous LIG at the top area of multistage structure can store a lot of air, which is in agreement with the Cassie–Baxter model. Meanwhile, as the focusing distance increases from 2 to 8 cm, the droplet is directly put in contact with the smooth surface at the top of jigsaw-like LIG. Without the secondary structure of porous LIG, there is no air captured at the solid–liquid interface, which is consistent with the Wenzel model.

To this end, two key factors of surface roughness and chemical composition were quantitatively analyzed to investigate the wetting mechanism of jigsaw-like structural LIG. As shown in Fig. 4a, the relationships between these geometrical parameters and d illustrate a clear linear trend, including top width (from 70.3 to 35.5 μm), bottom width (from 112.8 to 102.6 μm) and height (from 195.3 to 159.7 μm). Theoretically, the change of surface morphology causes roughness differences and is the key factor of surface wettability. In this regard, the following expression holds:

$$\cos\theta_{\omega} = r\cos\theta, \tag{2}$$

where θ_{ω} represents the apparent contact angle, r represents the roughness factor, and θ represents the intrinsic contact angle on an ideally smooth surface. This means that an increase in surface roughness enhances the inherent wetting state. As the distribution of bionic morphology becomes regular, the fluctuation of surface roughness gets smaller and more uniform. The root mean square roughness (R_q) of the top layer shows a linear trend, decreasing from 195.3 to 159.7 μm within the parameter range.

In order to highlight the effect of chemical composition on the surface wettability of jigsaw-like LIG, the full XPS spectra of samples fabricated with different d are displayed in Fig. S8 (Supplementary Information). With the decrease of d, the mass content of C reduces, and the O- and N-containing functional groups easily escaped, such that their mass contents were significantly increased. The related N/C and O/C ratios

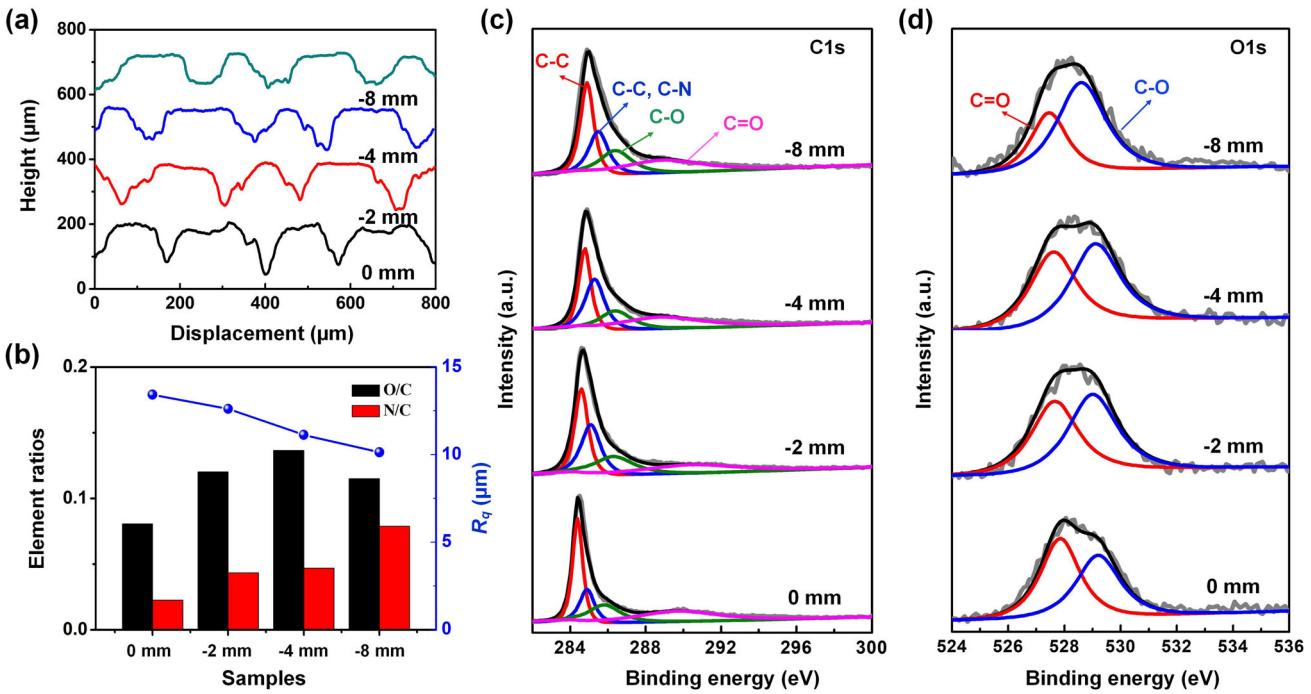

Fig. 4 The wetting properties of jigsaw-like structural LIG were quantitatively analyzed with changed surface roughness and chemical composition at different focusing distances: **a** The 3D topography curves of jigsaw-like units at displacement from 0 to 800 μm. The geometrical parameters of top width, bottom width and height showed a linear decreasing trend with the increase in focus distance from 2 to 4 mm and then 8 mm. **b** The element ratio of O/C and N/C, and the root mean square roughness (R_q) of the carbonized layer on a jigsaw-like unit. The high-resolution XPS spectra of **c** C1*s* and **d** O1*s* on the top area of bionic LIG

were calculated and shown in Fig. 4b. Moreover, the high-resolution XPS spectra of C1s indicated four typical carbon environments (Fig. 4c). The peak at 284.8 eV was assigned to the C–C bonds, the peak at 285.7 eV contained two different kinds of carbon atoms corresponding to C–C and C–N bonds, and the other two peaks at 286.8 eV and 288.6 eV were assigned to C–O bonds and C=O bonds, respectively. The degree of carbonization decreased with the increase of *d* because of the rise in C–C bonding ratio and decrease in C–N and C=O bonding ratios. These results suggest that many gases such as oxygen, carbon dioxide and nitrogen instantaneously escaped during the laser scribing of PI film.

As for the O1s spectra, two peaks at 532.5 eV and 533.6 eV were attributed to the C=O and C–O, respectively (Fig. 4d). These chemical bonds, with the increase of *d*, are less broken or released. The in situ growth of LIG and a series of phase transition processes, such as liquefaction and gasification, become relatively mild. The contact between jigsaw-like LIG and droplets under defocusing condition conforms to the Wenzel model. The decrease in surface roughness and carbonization degree is manifested by the reduction of polar functional groups, resulting in a slight decrease of WCAs on the bionic LIG. As reported in the previous works [5, 22], laser defocusing is an effective method to fine-tune the chemical composition and carbon structure of LIG, opening up a new pathway for the preparation of superhydrophobic surface.

Analysis of surface roughness and chemical composition

The surface wetting mechanism of jigsaw-like LIG is shown in Fig. 5a. In general, the presence of air can greatly reduce the solid/liquid contact area. The air layer in the porous LIG acts as a water-repellent, preventing water droplets from soaking the top area of jigsaw-like LIG and seeping into its bottom (Fig. 5b). Water droplets can then be lifted from surface and roll down effortlessly, mimicking the "lotus effect" and conforming to the Cassie–Baxter model. For the pinned state, the limited solid/surface contact area is partially wetted due to the lack of air fixation in porous LIG. The relatively high surface energy and smooth grooves of bionic LIG facilitate water droplet immersion. Similar to the "petal effect," the water–solid interface has a strong interaction, which conforms to the Wenzel model. These results indicate that the transition from the Cassie–Baxter model to the Wenzel model is related to surface roughness, geometric parameters (length, width, and height) and chemical composition (mass contents of C, N, and O).

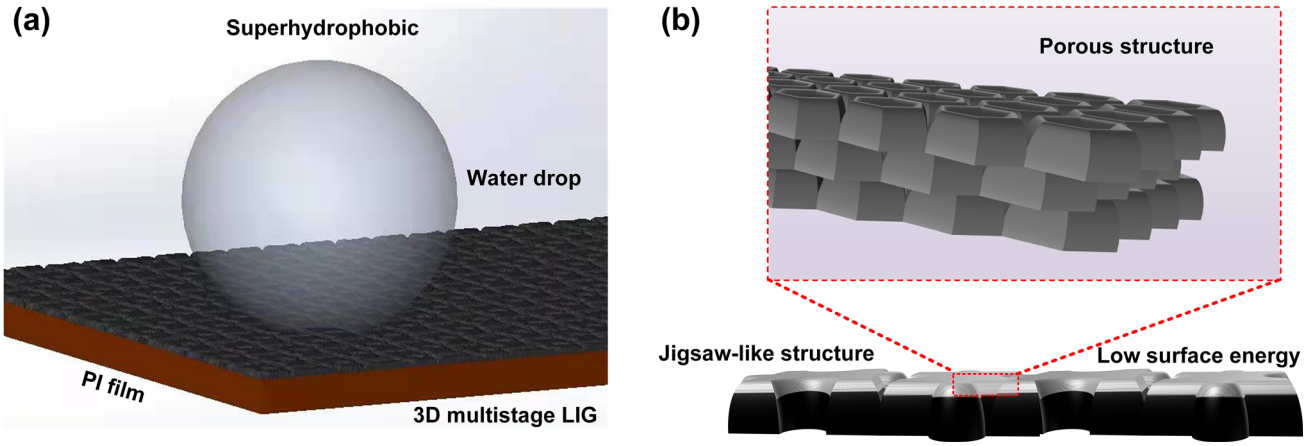

Fig. 5 **a** Schematic diagram of a superhydrophobic water droplet on a 3D jigsaw-like LIG. **b** The air layer in the 3D porous LIG acts as a water-repellent, preventing water droplets from soaking the top area and seeping into the bottom

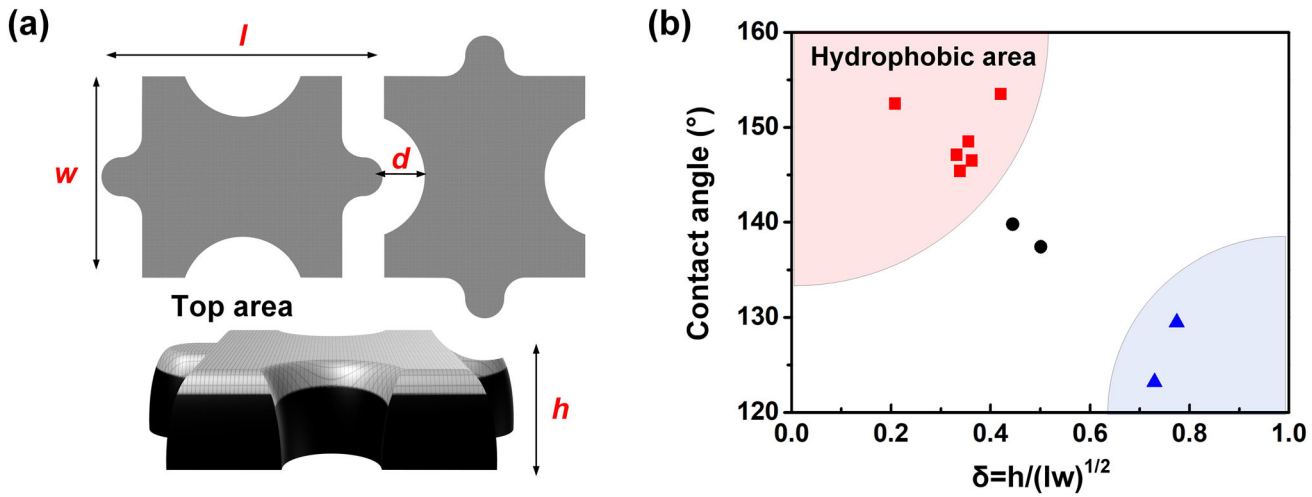

Fig. 6 **a** The geometric parameters of the jigsaw-like structural LIG, including height, length and width, as well as the distance between the adjacent units, are summarized to investigate the structure–wettability relationship. **b** The height/top area ratio of a typical jigsaw-like structure was calculated as a geometric factor (δ), and it was illustrated as a function of WCAs. The whole area can be divided into three parts, and most of the WCAs are greater than 145° when their δ value is < 0.43

By calculating the ratio of height to top area, we established the relationship between the geometric parameters and the wettability of jigsaw-like LIG. The top region of a typical bionic structural unit can be cut and calculated using a rectangular area (Fig. 6a). Accordingly, a geometric factor (δ) is introduced to describe the geometrical effects under different processing parameters, given by the following formula:

$$\delta = \frac{h}{\sqrt{lw}}, \tag{3}$$

where h, l, and w, respectively, represent the height, length and width of a jigsaw-like LIG unit. For each machining parameter, at least five units are selected to measure the geometric parameters. Another important physical parameter is marginal texture, which is related to the laser spot size, etching, and induction process. If the distance between the two bionic units is too large or too small, the wettability of jigsaw-like LIG will be close to that of pure LIG. The underlying mechanism requires in-depth investigation, which will be discussed in our future work.

In order to further investigate the potential relationships between geometric parameters and surface wettability, the WCAs of jigsaw-like LIG as a function of geometrical effects δ are summarized in Fig. 6b. We can see that the whole area can be divided into three parts. When δ is less than 0.43, most of the WCAs on bionic LIG are greater than 145°; on the contrary, when δ is greater than 0.6, the WCA of samples is less than 130°, which is similar to that of pure LIG. Through this simple description of the above-discussed

relationship, we can draw a basic conclusion: The wettability of jigsaw-like LIG is proportional to the height of bionic structure and is negatively correlated with the contact area between water droplet and top area. However, this is only a general statement because the effect of air layer in the top region is not considered if the solid–liquid interface conforms to the Cassie–Baxter model, and the subtle differences in surface roughness, and mass content of C, N and O are also ignored.

Surface wettability of bionic LIG

In addition to the above mechanism analysis, we also conducted a complete wettability test of the bionic surface. As shown in Fig. 7a, the surface wettability was firstly evaluated by water contact angle (WCA) measurements with about 5 μL deionized water (colorless) and other types of droplets, such as 20 wt% glucose solution (magenta), 20 wt% NaCl solution (brown), pure milk (white), artificial sweat (orange) and 20 wt% urea (purple). The CAs were measured at six different regions on each surface, and the average values are summarized in Fig. 7b. Most of these CAs showed superhydrophobic performance, including 153.5° ± 0.6° for deionized water, 150.5° ± 1.0° for pure milk, 151.5° ± 1.2° for NaCl solution, 150.3° ± 0.8° for glucose solution, 149.5° ± 1.6° for urea, and 146.7° ± 1.5° for artificial sweat.

Similar to the downward trend in these WCs, the sliding angle (SA) of deionized water droplets on the jigsaw-like LIG is the smallest at about 2.5° ± 0.4° (Video S1, Supplementary Information), and the SA of sweat is the largest at about 4.5° ± 1.8°. All the droplets are in a Cassie–Baxter state, indicating that the air layer plays a critical role in surface wetting. The subtle differences come from the surface energy and the intermolecular force between droplets and multistage LIG, which can be regarded as a chemical effect. The ability to bounce-off incoming droplets is also an important part of superhydrophobicity. Prior to recording, water droplets (5 μL) were released from a capillary by holding the tip about 50 mm away from the substrate (within an incline angle of 1°). As shown in Fig. 7c, the water droplets rapidly spread to the maximum shape after hitting the bionic LIG surface. The dynamic droplet then contracts into a strip that due to surface tension, springs back within a certain amount of time (Video S2, Supplementary Information). Due to inertia and gravity, after four round trips, the water droplets stay on the bionic surface without rolling down (the incline angle is less than the SA of 2.5° ± 0.4°), showing the excellent bounce-off ability and surface hydrophobicity of bionic LIG surface.

Furthermore, water droplets (about 5 μL) were gently placed on bionic LIG surfaces at room temperature to demonstrate the wettability evolution (Fig. 7d). The WCAs decreased slowly from about 152.0° to about 140.2° after 60 min. When the water droplet was placed at 110 °C, its volume decreased significantly in 15 min because of liquid evaporation, which is closely related to the coffee-stain effect. On the superhydrophobic surface of bionic LIG, the droplet is spherical, and its evaporation flux is relatively uniform. The visible difference between the wetting behavior of bionic LIG was measured at 0, 20, 40, 60, 80, and 100 days. We can see that the WCAs decreased slightly from about 152.1° (0 days) to about 149.5° (100 days), which is attributed to the gradual oxidation of the carbon structure. All CAs as a function of time are listed in Fig. 7e. As a result, we believe that the undesirable coffee-stain effect on bionic LIG is relatively weak, which is more conducive to medical applications. For example, human blood or saliva contains a large number of micro-/nanomolecules or biological particles, which can be precipitated using the coffee-stain effect and then used for biological detection and quantification. The coffee-stain effect occurs at the smallest size of particles, benefiting from the superhydrophobic LIG electrode, which can reduce the layout size of medical sensors. The technology relies entirely on liquid evaporation and does not require any complex structures, making the test facility cheap and easy-to-operate. In particular, in some remote areas without adequate medical equipment, medical electrodes fabricated with bionic LIG could greatly help to conduct relevant medical testing.

Dynamic wetting and self-cleaning properties

In order to evaluate the surface wettability of jigsaw-like LIG, the dynamic anti-stick application was demonstrated with an optimum bionic LIG sample (LHD of 0.05 J/mm, size of 200 μm, on-focus condition). As shown in Fig. 8a, water droplets are repelled rather than transferred to the surface when they come into contact with the bionic LIG. As the LIG sample is continuously immersed in water (methyl orange was added for comparison), the liquid is always repelled by the surface and cannot penetrate into the bionic structure. More importantly, water is squeezed to one side, presenting a clear solid–liquid boundary. As the sample is slowly raised from water, the droplet elongates due to surface adhesion and then completely detaches from the LIG surface.

During the whole dynamic anti-stick process, the bionic LIG surface is not wetted by residual water droplets (Video S3, Supplementary Information). According to the Cassie–Baxter theory, when a superhydrophobic surface comes into contact with a liquid, the air layer between the solid–liquid interface is critical. Here, the secondary structure of bionic LIG, which exhibits porous morphology, can form a thin air layer on the surface. The adhesion effect between the sample and water is significantly reduced, indicating that the bionic LIG with 3D multistage structure has strong hydrophobicity.

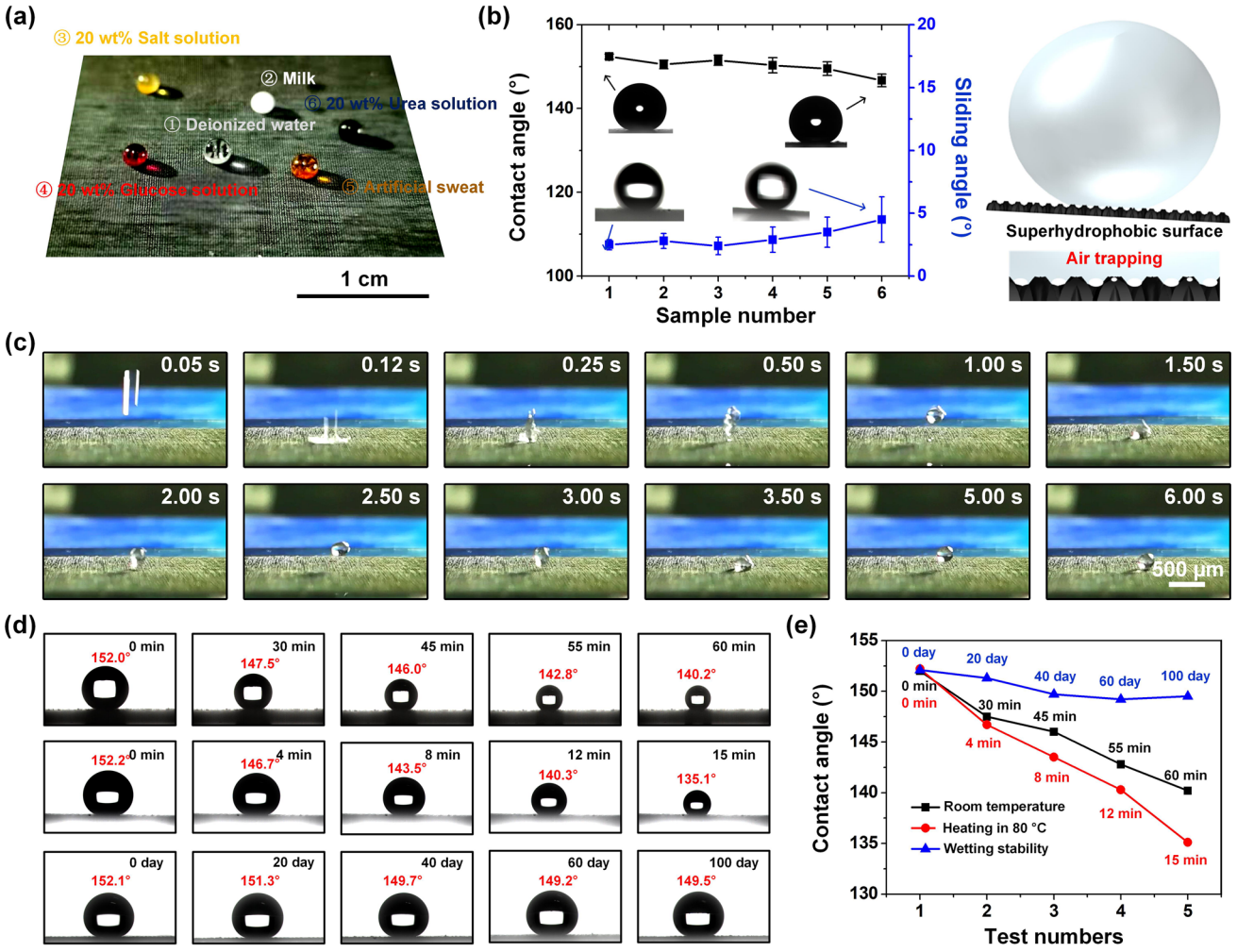

Fig. 7 **a** The wettability of the bionic LIG was evaluated by static CA measurements with about 5 μL deionized water (colorless), 20 wt% glucose solution (magenta), 20 wt% NaCl solution (brown), pure milk (white), artificial sweat (orange), and 20 wt% urea (purple). **b** Summary of static CAs and SAs of different kinds of droplets. **c** The incoming water droplet bounces four times by holding the tip 50 mm away from the substrate to demonstrate the outstanding superhydrophobicity of 3D multistage LIG. **d** Water droplets (about 5 μL) are gently placed on the bionic LIG surface at room temperature for 60 min and heated to 110 °C for 15 min. The surface superhydrophobicity lasts for up to 100 days (WCAs ≈ 150°). **e** The change of water repellency with time is summarized to show its stability on the surface

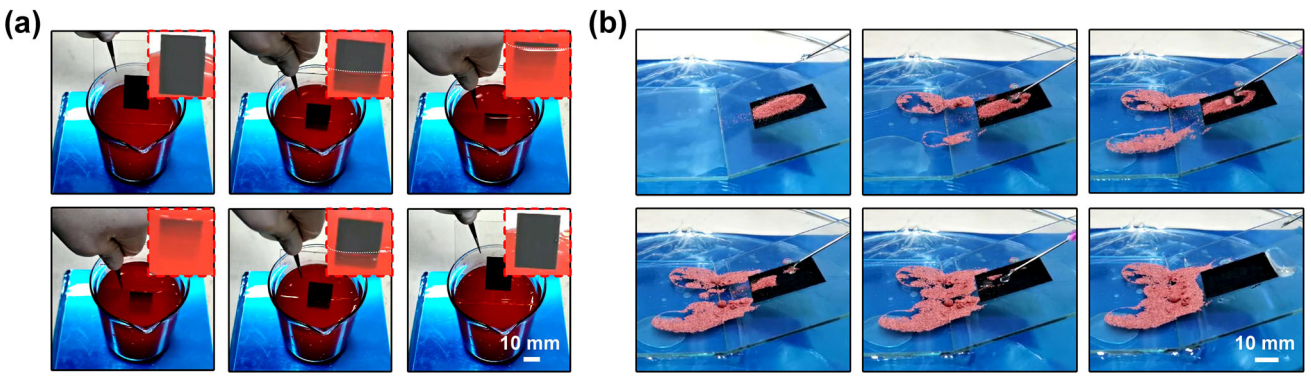

Fig. 8 **a** The bionic LIG is immersed in water without residual water droplets on its surface to demonstrate the dynamic anti-stick application value. **b** Water droplets continuously falling and washing away the copper powder on the bionic surface to demonstrate its self-cleaning feature

Next, we covered the surface of the bionic LIG with copper powder to demonstrate its self-cleaning ability. As shown in Fig. 8b, water is continuously squirted out of the needle. As the water droplets fall and wash away, the copper powder is carried away from the bionic surface. Finally, our sample surface becomes completely clean and not wetted with water droplets (Video S4, Supplementary Information). Thus, it is considered that the 3D multistage and jigsaw-like structure endows the bionic LIG superhydrophobic surface with excellent anti-pollution and self-cleaning performance. By laser scribing on some non-planar materials, bionic structures can be constructed on medical instruments through a simple, effective and on-demand approach, which is convenient for obtaining anti-stick and anti-dust properties. For instance, various artificial materials (blood vessels, scaffolds, prostheses, etc.) and surgical knives could stimulate blood to clot during surgery. To date, the main relevant method is to introduce low surface energy groups to adjust the hydrophilicity/hydrophobicity of medical materials, but these are often limited by poor biocompatibility. On the contrary, our method can be used to manufacture anticoagulant materials and devices at low cost and in large quantities, which is more conducive to commercialization and future clinical applications.

Conclusions

In this study, inspired by the hydrophobic properties of natural *Oxalis corniculata Linn.* leaves, a 3D multistage LIG consisting of micro-jigsaw-like structure and porous structure was laser-scribed on a non-planar PI film. The structure–wettability relationship between the 3D bionic surface was established in terms of size, topography (by controlling the laser power and focusing distance) and aspect ratio. The secondary structure of jigsaw-like LIG, which has porous morphology, can trap an air layer inside the solid–liquid interface, such that the bionic surface obtains outstanding water-repellent properties. Regardless of differences in the trapped air layer and the chemical composition, the surface wettability of bionic LIG is proportional to the height and is negatively correlated with the top area of a jigsaw-like unit. The 3D bionic structures prepared by this method can be further applied for the surface modification of biomedical materials and anti-adhesion properties of medical instruments.

Supplementary Information The online version contains supplementary material available at https://doi.org/10.1007/s42242-022-00197-0.

Acknowledgements The current study was supported by the Natural Science Foundation of Guangdong Province, China (No. 2021B1515020087) and the National Natural Science Foundation of China (No. 51905178).

Author contributions WTW: writing-original draft preparation. LSL: conceptualization, data curation. XYL: methodology. ZBL: investigation. BT: software. YXX: writing-reviewing and editing.

Declarations

Conflict of interest The authors declare that they have no conflict of interest.

Ethical approval This study does not contain any studies with human or animal subjects performed by any of the authors.

References

1. Chyan Y, Ye R, Li Y et al (2018) Laser-induced graphene by multiple lasing: toward electronics on cloth, paper, and food. ACS Nano 12:2176–2183. https://doi.org/10.1021/acsnano.7b08539
2. Ye R, James DK, Tour JM et al (2018) Laser-induced graphene. Acc Chem Res 51:1609–1620. https://doi.org/10.1021/acs.accounts.8b00084
3. Le TSD, Park S, An J et al (2019) Ultrafast laser pulses enable one-step graphene patterning on woods and leaves for green electronics. Adv Funct Mater 29:1902771. https://doi.org/10.1002/adfm.201902771
4. Gao J, Shao C, Shao S et al (2019) Laser-assisted multiscale fabrication of configuration-editable supercapacitors with high energy density. ACS Nano 13:7463–7470. https://doi.org/10.1021/acsnano.9b02176
5. Wang Y, Wang Y, Zhang P et al (2018) Laser-induced freestanding graphene papers: a new route of scalable fabrication with tunable morphologies and properties for multifunctional devices and structures. Small 14:1802350. https://doi.org/10.1002/smll.201802350
6. Wang W, Lu L, Xie Y et al (2020) Tailoring the surface morphology and nanoparticle distribution of laser-induced graphene/Co_3O_4 for high-performance flexible microsupercapacitors. Appl Surf Sci 504:144487. https://doi.org/10.1016/j.apsusc.2019.144487
7. Zhang C, Peng Z, Huang C et al (2021) High-energy all-in-one stretchable micro-supercapacitor arrays based on 3D laser-induced graphene foams decorated with mesoporous ZnP nanosheets for self-powered stretchable systems. Nano Energy 81:105609. https://doi.org/10.1016/j.nanoen.2020.105609
8. Zang X, Jian C, Zhu T et al (2019) Laser-sculptured ultrathin transition metal carbide layers for energy storage and energy harvesting applications. Nat Commun 10:3112. https://doi.org/10.1038/s41467-019-10999-z
9. Kulyk B, Silva BFR, Carvalho AF et al (2021) Laser-induced graphene from paper for mechanical sensing. ACS Appl Mater Interf 13:10210–10221. https://doi.org/10.1021/acsami.0c20270
10. Carvalho AF, Fernandes AJS, Leitão C et al (2018) Laser-induced graphene strain sensors produced by ultraviolet irradiation of polyimide. Adv Funct Mater 28:1805271. https://doi.org/10.1002/adfm.201805271
11. Li Y, Luong DX, Zhang J et al (2017) Laser-induced graphene in controlled atmospheres: from superhydrophilic to superhydrophobic surfaces. Adv Mater 29:1700496. https://doi.org/10.1002/adma.201700496
12. Wang WT, Lu LS, Xie YX et al (2020) A highly stretchable microsupercapacitor using laser-induced graphene/NiO/Co_3O_4 electrodes on a biodegradable waterborne polyurethane substrate. Adv Mater Technol 5:1900903. https://doi.org/10.1002/admt.201900903

13. Ye R, James DK, Tour JM et al (2019) Laser-induced graphene: from discovery to translation. Adv Mater 31:1803621. https://doi.org/10.1002/adma.201803621
14. Wang WT, Lu LS, Xie YX et al (2021) One-step laser induced conversion of a gelatin-coated polyimide film into graphene: tunable morphology, surface wettability and microsupercapacitor applications. Sci China Technol Sci 64:1030–1040. https://doi.org/10.1007/s11431-020-1609-4
15. Li JT, Stanford MG, Chen W et al (2020) Laminated laser-induced graphene composites. ACS Nano 14:7911–7919. https://doi.org/10.1021/acsnano.0c02835
16. Le Dinh TS, An J, Huang Y et al (2019) Ultrasensitive anti-interference voice recognition by bio-inspired skin-attachable self-cleaning acoustic sensors. ACS Nano 13:13293–13303. https://doi.org/10.1021/acsnano.9b06354
17. Luong DX, Yang K, Yoon J et al (2019) Laser-induced graphene composites as multifunctional surfaces. ACS Nano 13:2579–2586. https://doi.org/10.1021/acsnano.8b09626
18. Rafiee J, Rafiee MA, Yu ZZ et al (2010) Superhydrophobic to superhydrophilic wetting control in graphene films. Adv Mater 22:2151–2154. https://doi.org/10.1002/adma.200903696
19. Parmeggiani M, Zaccagnini P, Stassi S et al (2019) PDMS/Polyimide composite as an elastomeric substrate for multifunctional laser-induced graphene electrodes. ACS Appl Mater Interf 11:33221–33230. https://doi.org/10.1021/acsami.9b10408
20. Du Q, Liu J, Guo L et al (2016) Tailoring the surface wettability of polyimide by UV laser direct texturing in different gas atmospheres. Mater Des 104:134–140. https://doi.org/10.1016/j.matdes.2016.05.008
21. Wang Y, Wang G, He M et al (2021) Multifunctional laser-induced graphene papers with combined defocusing and grafting processes for patternable and continuously tunable wettability from superlyophilicity to superlyophobicity. Small 17:2103322. https://doi.org/10.1002/smll.202103322
22. Nasser J, Lin J, Zhang L et al (2020) Laser induced graphene printing of spatially controlled super-hydrophobic/hydrophilic surfaces. Carbon 162:570–578. https://doi.org/10.1016/j.carbon.2020.03.002
23. Jeong SY, Ma YW, Lee JU et al (2019) Flexible and highly sensitive strain sensor based on laser-induced graphene pattern fabricated by 355 nm pulsed laser. Sensors 19:4867. https://doi.org/10.3390/s19224867
24. Wang WT, Lu LS, Xie YX et al (2020) Controlling the laser induction and cutting process on polyimide films for kirigami-inspired supercapacitor applications. Sci China Technol Sci 64:651–661. https://doi.org/10.1007/s11431-019-1543-y
25. Xie H, Huang HX, Peng YJ et al (2017) Rapid fabrication of bio-inspired nanostructure with hydrophobicity and antireflectivity on polystyrene surface replicating from cicada wings. Nanoscale 9:11951–11958. https://doi.org/10.1039/c7nr04176d
26. Wang JN, Liu YQ, Zhang YL et al (2018) Wearable superhydrophobic elastomer skin with switchable wettability. Adv Funct Mater 28:1800625. https://doi.org/10.1002/adfm.201800625
27. Lou Z, Chen S, Wang L et al (2017) Ultrasensitive and ultraflexible e-skins with dual functionalities for wearable electronics. Nano Energy 38:28–35. https://doi.org/10.1016/j.nanoen.2017.05.024
28. Jung YH, Park B, Kim JU et al (2019) Bioinspired electronics for artificial sensory systems. Adv Mater 31:1803637. https://doi.org/10.1002/adma.201803637
29. Wong TS, Kang SH, Tang SKY et al (2011) Bioinspired self-repairing slippery surfaces with pressure-stable omniphobicity. Nature 477:443–447. https://doi.org/10.1038/nature10447
30. Barthlott W, Mail M, Bhushan B et al (2017) Plant surfaces: structures and functions for biomimetic innovations. Nano-Micro Lett 9:23. https://doi.org/10.1007/s40820-016-0125-1
31. Nine MJ, Tung TT, Alotaibi F et al (2017) Facile adhesion-tuning of superhydrophobic surfaces between "lotus" and "petal" effect and their influence on icing and deicing properties. ACS Appl Mater Interf 9:8393–8402. https://doi.org/10.1021/acsami.6b16444
32. Zheng Y, Zhang C, Wang J et al (2020) Nonwet kingfisher flying in the rain: the tumble of droplets on moving oriented anisotropic superhydrophobic substrates. ACS Appl Mater Interf 12:35707–35715. https://doi.org/10.1021/acsami.0c08889
33. Liu L, Jiao Z, Zhang J et al (2021) Bioinspired, superhydrophobic, and paper-based strain sensors for wearable and underwater applications. ACS Appl Mater Interf 13:1967–1978. https://doi.org/10.1021/acsami.0c18818
34. Park JK, Yang Z, Kim S et al (2017) Black silicon/elastomer composite surface with switchable wettability and adhesion between lotus and rose petal effects by mechanical strain. ACS Appl Mater Interf 9:33333–33340. https://doi.org/10.1021/acsami.7b11143
35. Xu R, Zverev A, Hung A et al (2018) Kirigami-inspired, highly stretchable micro-supercapacitor patches fabricated by laser conversion and cutting. Microsyst Nanoeng 4:36. https://doi.org/10.1038/s41378-018-0036-z
36. Tiliakos A, Ceaus C, Iordache SM et al (2016) Morphic transitions of nanocarbons via laser pyrolysis of polyimide films. J Anal Appl Pyrolysis 121:275–286. https://doi.org/10.1016/j.jaap.2016.08.007
37. Kim Y, Noh Y, Park S et al (2020) Ablation of polyimide thin-film on carrier glass using 355 nm and 37 ns laser pulses. Int J Heat Mass Transf 147:118896. https://doi.org/10.1016/j.ijheatmasstransfer.2019.118896
38. Lee JU, Ma YW, Jeong SY et al (2020) Direct fabrication of ultra-sensitive humidity sensor based on hair-like laser-induced graphene patterns. Micromachines 11:476. https://doi.org/10.3390/MI11050476
39. Hu S, Shi Z, Zheng R et al (2020) Superhydrophobic liquid-solid contact triboelectric nanogenerator as a droplet sensor for biomedical applications. ACS Appl Mater Interf 12:40021–40030. https://doi.org/10.1021/acsami.0c10097
40. Han Z, Wang Z, Li B et al (2019) Flexible self-cleaning broadband antireflective film inspired by the transparent cicada wings. ACS Appl Mater Interf 11:17019–17027. https://doi.org/10.1021/acsami.9b01948
41. Choong CL, Shim MB, Lee BS et al (2014) Highly stretchable resistive pressure sensors using a conductive elastomeric composite on a micropyramid array. Adv Mater 26:3451–3458. https://doi.org/10.1002/adma.201305182
42. Lee JU, Ma YW, Jeong SY et al (2020) Fabrication of UV laser-induced porous graphene patterns with nanospheres and their optical and electrical characteristics. Materials 13:3930. https://doi.org/10.3390/MA13183930
43. Lin N, Chen H, Wang W et al (2021) Laser-induced graphene/MoO_2 core-shell electrodes on carbon cloth for integrated, high-voltage, and in-planar microsupercapacitors. Adv Mater Technol 6:2000991. https://doi.org/10.1002/admt.202000991
44. Wang G, Wang Y, Luo Y et al (2020) A self-converted strategy toward multifunctional composites with laser-induced graphitic structures. Compos Sci Technol 199:108334. https://doi.org/10.1016/j.compscitech.2020.108334
45. Wang F, Wang K, Dong X et al (2017) Formation of hierarchical porous graphene films with defects using a nanosecond laser on polyimide sheet. Appl Surf Sci 419:893–900. https://doi.org/10.1016/j.apsusc.2017.05.084
46. Trusovas R, Ratautas K, Račiukaitis G et al (2019) Graphene layer formation in pinewood by nanosecond and picosecond laser irradiation. Appl Surf Sci 471:154–161. https://doi.org/10.1016/j.apsusc.2018.12.005

47. Go D, Lott P, Stollenwerk J et al (2016) Laser carbonization of PAN-nanofiber mats with enhanced surface area and porosity. ACS Appl Mater Interf 8:28412–28417. https://doi.org/10.1021/acsami.6b09358
48. Ruan X, Wang R, Luo J et al (2018) Experimental and modeling study of CO_2 laser writing induced polyimide carbonization process. Mater Des 160:1168–1177. https://doi.org/10.1016/j.matdes.2018.10.050
49. Wang R, Duan X, Yao J et al (2020) Processing–structure–property relationship in direct laser writing carbonization of polyimide. J Appl Polym Sci 137:e48978. https://doi.org/10.1002/app.48978
50. Zang X, Jian C, Ingersoll S et al (2020) Laser-engineered heavy hydrocarbons: old materials with new opportunities. Sci Adv 6:eaaz5231. https://doi.org/10.1126/sciadv.aaz5231